experiments in Fig. 5, the cultured microglia (see Supplementary Figure) that had been preincubated with or without ATP (50 μM) were injected intrathecally in normal rats (see Supplementary Methods for full details).

Immunohistochemistry

Transverse L5 spinal cord sections (30 μm) were cut and processed for immunohistochemistry with anti-P2X4R antibody (Alomone). Identification of the type of $P2X_4R$-positive cells was performed with the following markers: for microglia, OX42 (Chemicon) and iba1 (a gift from S. Kohsaka); for astrocytes, GFAP (Boehringer Mannheim); for spinal cord neurons, NeuN (Chemicon) and MAP2 (Chemicon). To assess immunofluorescence staining of cells quantitatively, we measured the immunofluorescence intensity of the $P2X_4R$ or OX42 as the average pixel intensity within each cell (see also Supplementary Methods).

Western blotting

Western blot analysis of $P2X_4R$ expression in the membrane fraction from L4–L6 spinal cord was performed with anti-P2X4R polyclonal antibody (Oncogene) as described in detail in the Supplementary Methods.

Microglial culture

Rat primary cultured microglia were prepared in accordance with the method described previously[28]. In brief, mixed glial culture was prepared from neonatal Wistar rats and maintained for 10–16 days in DMEM medium with 10% fetal bovine serum. Immediately before experiments, microglia were collected by a gentle shake as the floating cells over the mixed glial culture. The microglia were transferred to coverslips or to Eppendorf tubes for subsequent intrathecal administration.

Statistics

Statistical analyses of the results were made with Student's *t*-test, Student's paired *t*-test or the Mann–Whitney *U*-test.

Received 17 March; accepted 8 May 2003; doi:10.1038/nature01786.

1. Woolf, C. J. & Mannion, R. J. Neuropathic pain: Aetiology, symptoms, mechanisms, and management. *Lancet* **353,** 1959–1964 (1999).
2. Woolf, C. J. & Salter, M. W. Neuronal plasticity: Increasing the gain in pain. *Science* **288,** 1765–1769 (2000).
3. Bo, X., Zhang, Y., Nassar, M., Burnstock, G. & Schoepfer, R. A P2X purinoceptor cDNA conferring a novel pharmacological profile. *FEBS Lett.* **375,** 129–133 (1995).
4. Buell, G., Lewis, C., Collo, G., North, R. A. & Surprenant, A. An antagonist-insensitive P2X receptor expressed in epithelia and brain. *EMBO J.* **15,** 55–62 (1996).
5. Seguela, P., Haghighi, A., Soghomonian, J. J. & Cooper, E. A novel neuronal P2X ATP receptor ion channel with widespread distribution in the brain. *J. Neurosci.* **16,** 448–455 (1996).
6. Soto, F. *et al.* P2X4: an ATP-activated ionotropic receptor cloned from rat brain. *Proc. Natl Acad. Sci. USA* **93,** 3684–3688 (1996).
7. Wang, C. Z., Namba, N., Gonoi, T., Inagaki, N. & Seino, S. Cloning and pharmacological characterization of a fourth P2X receptor subtype widely expressed in brain and peripheral tissues including various endocrine tissues. *Biochem. Biophys. Res. Commun.* **220,** 196–202 (1996).
8. Khakh, B. S. *et al.* International union of pharmacology. XXIV. Current status of the nomenclature and properties of P2X receptors and their subunits. *Pharmacol. Rev.* **53,** 107–118 (2001).
9. Kim, S. H. & Chung, J. M. An experimental model for peripheral neuropathy produced by segmental spinal nerve ligation in the rat. *Pain* **50,** 355–363 (1992).
10. Virginio, C., Robertson, G., Surprenant, A. & North, R. A. Trinitrophenyl-substituted nucleotides are potent antagonists selective for $P2X_1$, $P2X_3$, and heteromeric $P2X_{2/3}$ receptors. *Mol. Pharmacol.* **53,** 969–973 (1998).
11. Tsuda, M., Ueno, S. & Inoue, K. Evidence for the involvement of spinal endogenous ATP and P2X receptors in nociceptive responses caused by formalin and capsaicin in mice. *Br. J. Pharmacol.* **128,** 1497–1504 (1999).
12. Zheng, J. H. & Chen, J. Modulatory roles of the adenosine triphosphate P2X-purinoceptor in generation of the persistent nociception induced by subcutaneous bee venom injection in the conscious rat. *Neurosci. Lett.* **278,** 41–44 (2000).
13. Tsuda, M., Ueno, S. & Inoue, K. *In vivo* pathway of thermal hyperalgesia by intrathecal administration of α,β-methylene ATP in mouse spinal cord: Involvement of the glutamate-NMDA receptor system. *Br. J. Pharmacol.* **127,** 449–456 (1999).
14. Honore, P. *et al.* Murine models of inflammatory, neuropathic and cancer pain each generates a unique set of neurochemical changes in the spinal cord and sensory neurons. *Neuroscience* **98,** 585–598 (2000).
15. Aldskogius, H. & Kozlova, E. N. Central neuron–glial and glial–glial interactions following axon injury. *Prog. Neurobiol.* **55,** 1–26 (1998).
16. Sawynok, J., Downie, J. W., Reid, A. R., Cahill, C. M. & White, T. D. ATP release from dorsal spinal cord synaptosomes: Characterization and neuronal origin. *Brain Res.* **610,** 32–38 (1993).
17. Li, P., Calejesan, A. A. & Zhuo, M. ATP P2X receptors and sensory synaptic transmission between primary afferent fibers and spinal dorsal horn neurons in rats. *J. Neurophysiol.* **80,** 3356–3360 (1998).
18. Nakatsuka, T. & Gu, J. G. ATP P2X receptor-mediated enhancement of glutamate release and evoked EPSCs in dorsal horn neurons of the rat spinal cord. *J. Neurosci.* **21,** 6522–6531 (2001).
19. Bardoni, R., Goldstein, P. A., Lee, C. J., Gu, J. G. & MacDermott, A. B. ATP P2X receptors mediate fast synaptic transmission in the dorsal horn of the rat spinal cord. *J. Neurosci.* **17,** 5297–5304 (1997).
20. Jo, Y. H. & Schlichter, R. Synaptic corelease of ATP and GABA in cultured spinal neurons. *Nature Neurosci.* **2,** 241–245 (1999).
21. Fam, S. R., Gallagher, C. J. & Salter, M. W. $P2Y_1$ purinoceptor-mediated Ca^{2+} signaling and Ca^{2+} wave propagation in dorsal spinal cord astrocytes. *J. Neurosci.* **20,** 2800–2808 (2000).
22. Inoue, K. Microglial activation by purines and pyrimidines. *Glia* **40,** 156–163 (2002).
23. Hanisch, U. K. Microglia as a source and target of cytokines. *Glia* **40,** 140–155 (2002).
24. Vitkovic, L., Bockaert, J. & Jacque, C. 'Inflammatory' cytokines: Neuromodulators in normal brain? *J. Neurochem.* **74,** 457–471 (2000).
25. Nakajima, K. & Kohsaka, S. Functional roles of microglia in the brain. *Neurosci. Res.* **17,** 187–203 (1993).
26. Carson, M. J. Microglia as liaisons between the immune and central nervous systems: Functional implications for multiple sclerosis. *Glia* **40,** 218–231 (2002).
27. Eikelenboom, P. *et al.* Neuroinflammation in Alzheimer's disease and prion disease. *Glia* **40,** 232–239 (2002).
28. Nakajima, K. *et al.* Identification of elastase as a secretory protease from cultured rat microglia. *J. Neurochem.* **58,** 1401–1408 (1992).

Supplementary Information accompanies the paper on **www.nature.com/nature**.

Acknowledgements We thank J. Hicks for corrections to the manuscript. This work was supported by a Domestic Research Fellowship from the Japan Science and Technology Corporation, by a grant from the Uehara Memorial Foundation, partly by a grant from the Organization for Pharmaceutical Safety and Research, by a grant-in-aid for the scientific research from the Ministry of Education, Science, Sports, and Culture of Japan, and by a grant from the Japan Health Sciences Foundation. M.T. is supported by the Research Training Centre of the Hospital for Sick Children Research Institute. M.W.S. is an Investigator of the Canadian Institutes of Health Research.

Competing interests statement The authors declare that they have no competing financial interests.

Correspondence and requests for materials should be addressed to K.I. (inoue@nihs.go.jp).

A camelid antibody fragment inhibits the formation of amyloid fibrils by human lysozyme

Mireille Dumoulin[1], Alexander M. Last[2], Aline Desmyter[3]*, Klaas Decanniere[3], Denis Canet[2]*, Göran Larsson[1], Andrew Spencer[4], David B. Archer[5], Jurgen Sasse[6], Serge Muyldermans[3], Lode Wyns[3], Christina Redfield[2], André Matagne[7], Carol V. Robinson[1] & Christopher M. Dobson[1]

[1]*Department of Chemistry, University of Cambridge, Lensfield Road, Cambridge CB2 1EW, UK*
[2]*Oxford Centre for Molecular Sciences, University of Oxford, South Parks Road, Oxford OX1 3QH, UK*
[3]*Department Ultrastructure, Vrije Universiteit Brussel, Pleinlaan 2, B-1050 Brussels, Belgium*
[4]*Institute of Food Research, Norwich Research Park, Colney, Norwich NR4 7UA, UK*
[5]*School of Life and Environmental Sciences, University of Nottingham, University Park, Nottingham NG7 2RD, UK*
[6]*Central Veterinary Research Laboratory, P.O. Box 597, Dubai, United Arab Emirates*
[7]*Laboratoire d'Enzymologie, Centre d'Ingénerie des Protéines, Institut de Chimie B6, Université de Liège, B-4000 Liège (Sart Tilman), Belgium*

* Present addresses: Centre National de la Recherche Scientifique, 31 Chemin Joseph Aiguier, 13402 Marseille, France (A.D.); Gene Prot Inc., 2 Pré-de-la-Fontaine, 1217 Meyrin/GE, Switzerland (D.C.)

Amyloid diseases are characterized by an aberrant assembly of a specific protein or protein fragment into fibrils and plaques that are deposited in various organs and tissues[1–3], often with serious pathological consequences. Non-neuropathic systemic amyloidosis[4–6] is associated with single point mutations in the gene coding for human lysozyme. Here we report that a single-domain fragment of a camelid antibody[7–9] raised against wild-type human lysozyme inhibits the *in vitro* aggregation of its amyloidogenic variant, D67H. Our structural studies reveal that the epitope includes neither the site of mutation nor most residues in the region of the protein structure that is destabilized by the mutation. Instead, the binding of the antibody fragment achieves its effect by restoring the structural cooperativity characteristic

of the wild-type protein. This appears to occur at least in part through the transmission of long-range conformational effects to the interface between the two structural domains of the protein. Thus, reducing the ability of an amyloidogenic protein to form partly unfolded species can be an effective method of preventing its aggregation, suggesting approaches to the rational design of therapeutic agents directed against protein deposition diseases.

Four mutations in the lysozyme gene (I56T, F57I, W74R, and D67H) have so far been identified in connection with amyloid disease[4–6]. The ability of the lysozyme variants studied in detail (I56T and D67H) to form amyloid deposits has been attributed primarily to their reduced stability relative to the wild-type protein, allowing transient unfolding of a local region of structure under physiologically relevant conditions[10,11]. The formation of partly structured species through this locally cooperative unfolding process appears to be the critical event that triggers the aggregation process and ultimately leads to the formation of amyloid fibrils and the onset of disease[11].

The use of specific antibodies is a promising strategy for inhibiting and even reversing *in vitro* and *in vivo* fibril formation by amyloidogenic peptides or proteins[12–14]. We focus here on the interaction of cAb-HuL6 (ref. 7), a fragment from a 'heavy-chain' camel antibody with high specificity for native human lysozyme and its amyloidogenic variants. Because antibodies derived from camelids (camels, dromedaries and llamas) are devoid of the light chains of conventional antibodies, their antigen binding sites are limited to single domains, referred to as V_HHs[8]. Such domains have very favourable properties[7–9] for biophysical studies, including small size and high solubility and stability.

To investigate the effects of the antibody fragment on fibril formation, conditions were selected (48 °C, pH 5.5, 3 M urea) under which the D67H variant readily aggregates *in vitro* while the antibody fragment remains stable and is still able to bind tightly to native lysozyme. In the absence of the antibody fragment, the data show that the D67H variant readily aggregates (Fig. 1a). The kinetics follow a sigmoidal curve consistent with the nucleation-dependent growth model that has been suggested as a common mechanism of fibril formation[15]. After incubation for 6 h, the protein solution was passed through a 0.22 μm filter and examined by SDS–polyacrylamide gel electrophoresis (SDS–PAGE). No protein could be detected on the gel (Fig. 1b, lane 4), indicating that virtually all the D67H protein had aggregated to form species too large to pass through the filter; the slight increase in light scattering observed over longer incubation times (6–15 h, Fig. 1a) is likely to result from the organization of the aggregates into higher-order structures. In contrast, when wild-type lysozyme was incubated under the same conditions, it remained almost completely soluble even after 20 h (Fig. 1a, b).

The aggregated species formed by the D67H variant under the conditions described above bind Congo red, producing the characteristic red shift in the absorption spectrum of the dye typically observed during amyloid fibril formation[16]. The presence of large quantities of fibrillar material was unambiguously confirmed by negative-stain transmission electron microscopy (TEM) (Fig. 1c). The structures observed include some well-resolved isolated fibrils (approximately 6 nm in diameter) although most fibrils appear to be incorporated into large bundles (100–400 nm in diameter). Such structures have previously been observed with a variety of other amyloidogenic proteins[17], including the I56T variant of human lysozyme after incubation at pH 2 and 37 °C (ref. 18). Moreover, the X-ray fibre diffraction pattern of the fibrils (Fig. 1d) shows a dominant meridional reflection at 4.7 Å and an equatorial reflection at 10.4 Å, features characteristic of amyloid fibrils as a consequence of their cross-β structure[19].

When the D67H protein was incubated in the presence of an equimolar amount of the antibody fragment, no significant changes in light scattering were detectable after 6 h of incubation (Fig. 1a), and after passage of the solution through a 0.22 μm filter, SDS–PAGE confirmed that virtually all of the D67H protein incubated with the antibody fragment remained in solution (Fig. 1b, lane 6). Finally, TEM analysis showed no evidence for the presence of amyloid fibrils or other aggregates. Thus, in the presence of an equimolar quantity of antibody fragment, the D67H variant behaves very similarly to the wild-type protein in the absence of the antibody fragment. Moreover, the rate of aggregation of the D67H protein in the presence of the antibody fragment can be estimated to be reduced by a factor of at least 100 relative to that in its absence. In the presence of a sub-stoichiometric amount of the antibody fragment (a D67H:cAb-HuL6 ratio of 1:0.5), the initial rate of aggregation of the D67H variant was reduced by a factor of approximately 3 (Fig. 1a). Then, after about 50% of the protein had formed aggregates, the remainder aggregated even more slowly, presumably at a rate limited by the rate of dissociation of the D67H protein from the complex. These observations provide clear evidence that the binding of the antibody fragment to the variant protein is directly responsible for the dramatic decrease in its rate of aggregation.

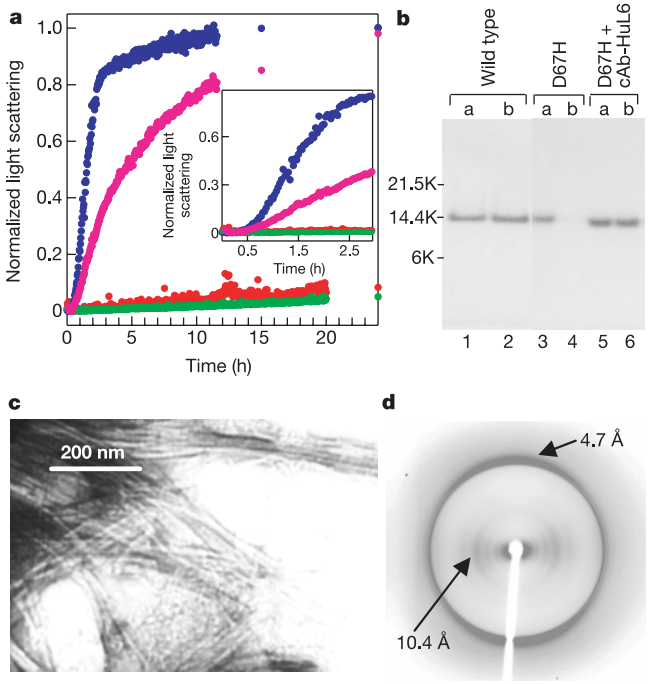

Figure 1 Effect of cAb-HuL6 on the aggregation of D67H lysozyme. **a**, Time course of the aggregation of D67H lysozyme in the absence (blue) and presence of the antibody fragment (D67H:cAb-HuL6 1:1 (green), D67H:cAb-HuL6 1:0.5 (pink)) monitored by light scattering. Data are also shown for wild-type lysozyme in the absence of cAb-HuL6 (red). Inset, expansion to demonstrate the lag phase at the onset of the aggregation process. **b**, SDS–PAGE of protein solutions filtered through a 0.22 μm filter before incubation at 48 °C (series a) and after 6 h of incubation at 48 °C (series b). Note that the D67H lysozyme and the cAb-HuL6 have similar relative molecular masses (14,715 and 14,220, respectively) and thus they migrate in closely similar position in lanes 5 and 6. The comparable intensities of the bands before and after heating suggest that both proteins remain soluble after treatment; this result was confirmed by measuring the protein concentration in the supernatant, using the BCA assay. **c**, Representative image of fibrils formed from the D67H variant produced by TEM. **d**, X-ray fibre diffraction pattern of the fibrils showing a prominent meridional reflection at 4.7 Å and an equatorial reflection at 10.4 Å, features typical of amyloid fibrils as a result of their cross-β structure. The additional equatorial reflections observed at 7.8 Å and 13.8 Å may arise from the superposition of interference functions as a consequence of the close packing of protofilaments[19].

Thermal denaturation experiments followed by far-ultraviolet circular dichroism measurements under the buffer conditions in which the uncomplexed D67H variant forms fibrils indicate that the temperature of the mid-point of unfolding of the D67H variant ($T_m = 55 \pm 1\,°C$) is reduced by about 10 °C compared with that of the wild-type protein, ($T_m = 65 \pm 1\,°C$). In the presence of an equimolar amount of the antibody fragment, however, the stability of the variant protein is raised by about 15 °C ($T_m = 70 \pm 1\,°C$). Within the complex, therefore, the thermal stability of the D67H lysozyme is even greater than that of the wild-type protein in the absence of the antibody fragment. Furthermore, thermally induced denaturation of the D67H variant was observed to be associated with a significant increase in the fluorescence intensity of 8-anilino-1-naphthalene-sulphonic acid (ANS) at 475 nm (data not shown), indicating that a partly unfolded intermediate species with one or more hydrophobic regions exposed to the solvent is significantly populated during unfolding. A similar enhancement of ANS fluorescence was not observed, however, in the presence of the antibody fragment. These data suggest that in the presence of the antibody fragment the D67H variant unfolds in a single cooperative two-state transition.

Further insight into the dynamics and structural cooperativity of the amyloidogenic D67H variant in the presence of the antibody fragment was gained from hydrogen/deuterium exchange pulse-labelling experiments analysed by mass spectrometry[11]. The bimodal mass distribution observed with the D67H protein as exchange takes place (Fig. 2a) is indicative of the transient cooperative unfolding of a local region of the structure shown previously to consist of the β-domain and the adjacent C-helix[11]. The time course of the intensity of the peak corresponding to the lower mass species in Fig. 2a provides a direct measure of the opening rate of the cooperative fluctuation giving rise to exchange (Fig. 2a inset); the time constant (τ) of 15.3 ± 0.6 s obtained from this analysis is consistent with earlier data obtained at higher pH values[11]. Most significantly, however, the peak that is observed at lower mass in the absence of the antibody fragment (coloured yellow in Fig. 2a) is not observed in the spectrum when an equimolar amount of the antibody fragment is present (Fig. 2b). Instead, the D67H protein gives rise to a single peak whose mass progressively decreases with time, an observation indicative of the gradual exchange of the various labile deuterons in the protein. Similar behaviour has been observed with the wild-type protein in the absence of the antibody fragment and results from amide hydrogens undergoing exchange through highly localized independent fluctuations of the structure[11].

These observations demonstrate that, in the presence of an equimolar amount of the antibody fragment, virtually none of the molecules of the D67H variant undergoes even a single locally cooperative unfolding event on the timescale of the experiment (about 1 h). This result indicates that the frequency of such fluctuations in the D67H variant is reduced by a factor of at least 2,000 as a result of binding to the antibody fragment. The presence

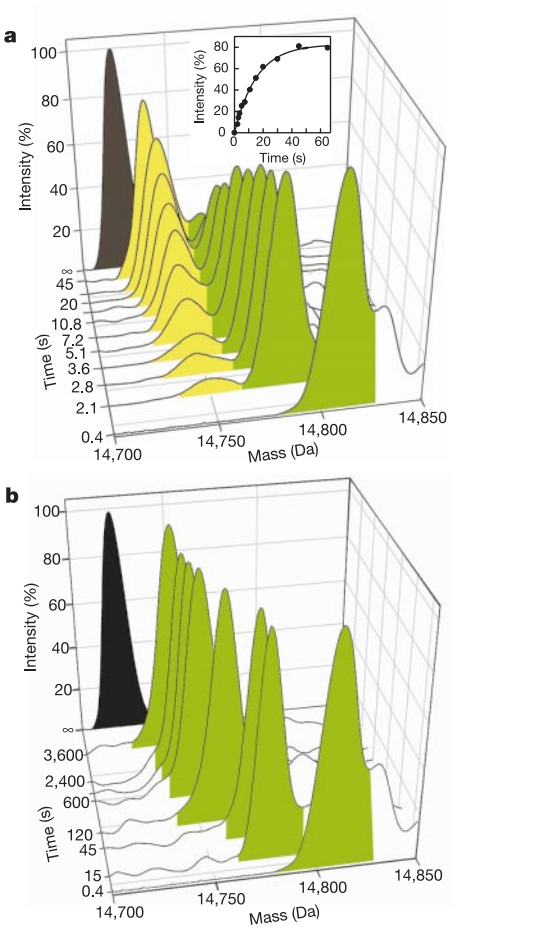

Figure 2 Electrospray mass spectra of D67H lysozyme in the absence (**a**) and presence (**b**) of an equimolar amount of cAb-HuL6. The peaks observed in spectra of control samples recorded after complete hydrogen–deuterium exchange are coloured black. The peaks coloured green arise from the gradual loss of deuterium during the course of the exchange reaction that occurs by an EX2 mechanism[11]. The peaks coloured yellow are observed in the spectra of the D67H variant in the absence of the antibody fragment but not in its presence. They result from the locally cooperative unfolding event giving rise to exchange by an EX1 mechanism[11]. Note the difference in the timescale between **a** and **b**. Inset in **a**, time course of the relative intensity of the lower mass species (peaks coloured yellow) observed for the unbound D67H variant (Fig. 2a). Fitting these data to an exponential function indicates that the time constant of the unfolding process is 15.3 ± 0.6 s.

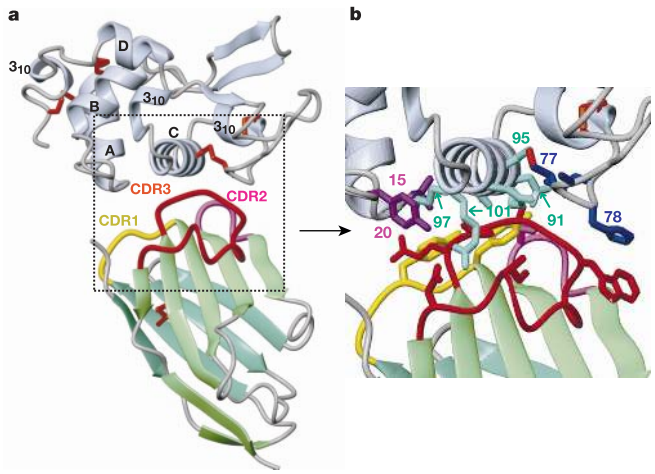

Figure 3 X-ray structure of wild-type human lysozyme complexed with cAb-HuL7. **a**, Ribbon representation of the complex. The β-strands in cAb-HuL6 are coloured green. The lysozyme molecule is shown in grey and the helices are labelled. The disulphide bridges are coloured orange. **b**, Enlarged view of the binding interface (that is, the area in the box in **a**). The side chains of residues constituting the epitope are shown in violet, light blue and dark blue for the α-domain, C-helix and β-domain of lysozyme, respectively. Those residues constituting the paratope are shown in yellow, pink and red, and are from the CDR1, CDR2 and CDR3 loops of the V_HH structure, respectively. The structure was produced by using MOLMOL (ref. 30).

of a stoichiometric amount of a V_HH that does not interact with lysozyme, cAb-R2[7], was found to have no effect on the dynamics of the D67H variant confirming that it is the specific binding of the cAb-HuL6 that is responsible for the inhibition of the partial unfolding event. The data from these various experiments, therefore, provide evidence that the formation of partly unstructured species, resulting from the locally cooperative unfolding of the β-domain and the C-helix is the critical event that triggers the aggregation process in the absence of the antibody fragment. Moreover, the results show that binding to the antibody fragment not only increases the overall stability of the D67H variant to a value even greater than that of the wild-type protein, but also reverses the loss of global structural cooperativity that results from the mutation.

To investigate in greater detail the structural basis for the efficacy of the antibody fragment as an inhibitor of the formation of amyloid fibrils, the complex with wild-type lysozyme was crystallized and the structure solved at a resolution of 1.8 Å by using X-ray diffraction (Fig. 3). Comparison of this structure with those available for unbound lysozyme reveals that no significant conformational changes result from the complexation of the protein to the antibody fragment; the Cα r.m.s. deviations of the lysozyme molecule in the complex from that of the uncomplexed species (pdb entries 1LZ1, 1REX and 1JWR) are all less than 0.4 Å. The structure of the complex reveals that the epitope consists of 14 residues of the lysozyme molecule and encompasses residues located in the loop between the A and B helices in the α-domain (L15, G16, Y20), in the long loop within the β-domain (A76, C77, H78, L79) and in the C-helix (A90, D91, A94, C95, K97, R 98, R101) (Fig. 3); binding of the antibody fragment results in a surface coverage in these regions of about 100 $Å^2$, 165 $Å^2$ and 305 $Å^2$, respectively. Thus, the C-helix contributes about half of the total surface area of the enzyme that is bound to the antibody fragment.

We performed NMR experiments to characterize further the interaction in solution between the wild-type and variant lysozyme molecules and the antibody fragment. Comparison of the ^{15}N-^{1}H heteronuclear single quantum coherence (HSQC) NMR spectra of the unbound proteins, uniformly labelled with ^{15}N, with spectra of the proteins complexed to an unlabelled antibody fragment allowed the binding region to be probed in a site-specific manner by analysis of the chemical shift perturbations of the resonances of the amide groups of individual residues. This analysis reveals that the resonances of approximately the same number of residues in the spectra of the wild-type lysozyme and the D67H variant (31 and 29, respectively) exhibit a significant chemical shift perturbation upon binding to the antibody fragment in solution (Fig. 4). Resonances of all the lysozyme residues found to be in direct contact with the antibody fragment in the X-ray structure were observed to be significantly shifted relative to their positions in the uncomplexed protein. Most of the additional residues with perturbed chemical shifts are located in close proximity to those that are in direct contact with the antibody fragment. Moreover, it is evident that the epitope is essentially identical in the D67H variant as in wild-type lysozyme. This last finding is consistent with the very

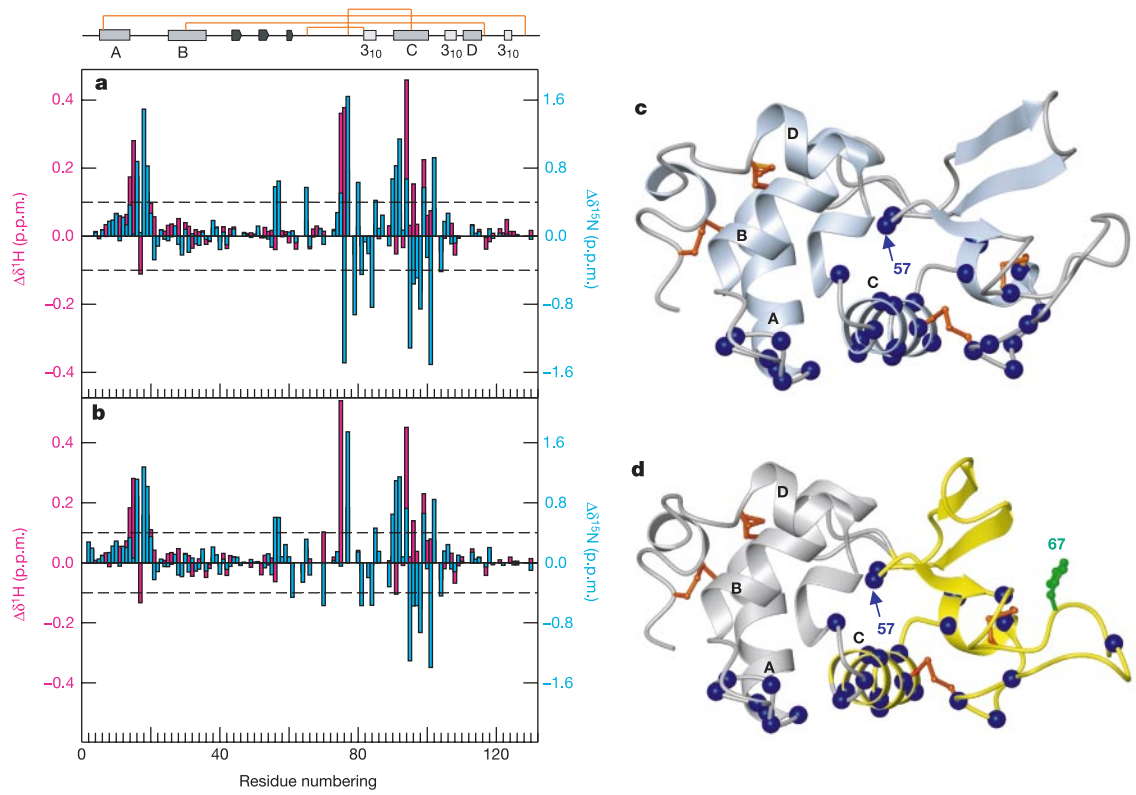

Figure 4 Chemical shift perturbations induced by the binding of the cAb-HuL6 to wild-type lysozyme (**a**) and the D67H variant (**b**). The pink and blue bars indicate the chemical shift perturbations of the ^{1}H and ^{15}N resonance, respectively; residues experiencing a chemical shift change of not less than ±0.4 p.p.m. for ^{15}N or not less than ±0.1 p.p.m. for ^{1}H resonances are considered to be significantly affected by the binding of the antibody fragment. The Cα atoms of these residues are shown in a blue space-filling representation on the ribbon diagram (**c**, wild-type lysozyme; **d**, D67H variant). The peaks corresponding to residues 76, 78 and 79 in the D67H-cAbHuL6 complex and to residue 78 in the wild-type protein complex have not been assigned; therefore shift differences for these peaks are not shown in the histograms. No unassigned peaks are visible in the spectra of either complex within 0.1 p.p.m. (^{1}H) and 0.4 p.p.m. (^{15}N) of the peak positions of residue 78 in the spectra of the unbound proteins. This finding strongly suggests that large shift perturbations are observed for this residue in both complexes. In **d**, the region of the D67H molecule that has been found to unfold transiently in a locally cooperative manner[11] is coloured yellow, and the amyloidogenic mutation D67H is indicated in green.

similar values of the dissociation constants for binding of the antibody fragment to wild-type lysozyme ($K_D = 0.7$ nM (ref. 7)) and the D67H variant ($K_D = 1.2$ nM, this work).

The crystal structure of the complex indicates that the antibody fragment binds to the C-terminal region of the long loop of the β-domain and to the C-helix of the α-domain of lysozyme. Remarkably, these are two of the elements of secondary structure that are destabilized by the D67H amyloidogenic mutation as a result of the disruption of the interface between the α- and β-domains[10,11] (Fig. 4d). This result therefore provides a ready explanation for the ability of the antibody fragment to prevent the partial unfolding and subsequent aggregation of the D67H variant. More detailed analysis, however, reveals that only 11 of the nearly 60 residues involved in the transient unfolding of the D67H variant are in direct contact with the antibody fragment. Thus, the effects of binding are not simply to mask the entire region of the protein destabilized by the mutation and hence to prevent its unfolding from the remainder of the structure. Rather, it appears that the binding of the antibody fragment restores the global cooperativity of the lysozyme structure that is disrupted by the D67H mutation by a more subtle mechanism. It is therefore of particular interest that perturbations to the NMR chemical shifts, reflecting small changes in the protein structure, include the amide resonances of residues 56 and 57, both of which are far from the site of mutation and from the binding interface with the antibody. In the crystal structure of the D67H variant it was found that the mutation disrupts the hydrogen bond network present in the β-domain of the wild-type protein, and that the resulting small conformational changes are transmitted to the region of the structure where residue 56 is located[10]. Moreover, residues 56 and 57 are themselves the locations of two of the other well-defined pathogenic mutations of lysozyme that give rise to amyloid disease[4,6].

As the result of the increasingly serious impact of amyloid diseases such as Alzheimer's and Parkinson's on the ageing populations of the developed world, a wide range of strategies for the prevention or treatment of these diseases is being very actively explored[20–24]. One of the most attractive therapeutic options is to prevent the accumulation of aggregation-prone species by inhibiting the processes that lead to their formation[23]. Studies of transthyretin, for example, have shown that small molecules mimicking the binding of natural ligands are highly promising therapeutic agents because they stabilize the native state of the protein, in this case a tetramer, by binding at the interface between the subunits and preventing their dissociation under physiological conditions[25,26]. We have shown here that a specific antibody fragment can achieve a similar effect in reducing the concentration of a partly unfolded aggregation-prone species, but in this case by stabilizing the interactions between distinct sub-structures of a monomeric protein. Unlike the situation with transthyretin, stabilization and inhibition of lysozyme aggregation does not occur as a result of binding at a site that is normally occupied by a natural ligand. Rather, it occurs through the restoration of the global cooperativity of the native structure, disrupted by the amyloidogenic mutation that is a consequence of the binding interaction. The region of the protein surface that forms the epitope of the antibody fragment does not include the site of the disruptive mutation; the antibody fragment thus acts through transmitted conformational changes in a manner that is in some respect analogous to the way in which binding of an effector molecule can regulate an allosteric protein[27]. This suggests that exploration of a series of antibodies raised against a given protein antigen could well allow the discovery of species able to overcome the effects of a wide range of pathogenic mutations, or indeed to stabilize a wild-type protein without disruption of the binding site or sites that are essential to its function. The properties of single domain fragments of camelid antibodies may make humanized versions of these molecules particularly favourable for such a purpose[9]. □

Methods

Proteins

Wild-type human lysozyme and its D67H variant, including uniformly [^{15}N]proteins, cAb-R2 and the cAb-HuL6 were expressed and purified as described previously[7,28]. The affinity of cAb-HuL6 for the two forms of lysozyme was determined by using surface plasmon resonance[7].

Thermal unfolding monitored by circular dichroism and fluorescence measurements

Thermal unfolding experiments were done in 0.1 M citrate buffer pH 5.5 containing 3 M urea, by raising the temperature from 5 to 75–95 °C at a rate of 0.5 °C min^{-1}. The far ultraviolet circular dichroism signal was monitored at 228 nm by using a Jasco J-810 spectropolarimeter with a 0.1-cm path-length cell using lysozyme concentrations of 13.5 μM. At this wavelength the signal arising from the antibody fragment is very low compared with that of lysozyme[7]. The changes in signal amplitude as a result of unfolding of the antibody fragment are therefore negligible, making it possible to monitor specifically the unfolding of lysozyme in the presence of cAb-HuL6. ANS-binding fluorescence emission data were recorded on a Cary Eclipse spectrofluorimeter. The excitation and emission wavelengths were 350 nm and 475 nm, respectively, and the slit widths were 5 nm. The lysozyme concentration was 2.5 μM in a 1-cm path-length cuvette and the final ANS concentration was 160 μM. For the experiments in the presence of the antibody fragment, equimolar amounts of cAb-HuL6 and D67H lysozyme were mixed immediately before the experiment.

Aggregation monitored by right-angle light scattering

Stock solutions of the proteins were prepared from lyophilized material, passed through a 0.22 μm filter, diluted to the desired final concentration into 0.1 M citrate buffer pH 5.5 containing 3 M urea and incubated at 48 °C with stirring in a Cary Eclipse spectrofluorimeter. The excitation wavelength was 500 nm and changes in fluorescence emission were monitored at 500 nm with slit widths of 5 nm. Aliquots of the samples after 6 h of incubation were centrifuged for 15 min at 15,000 *g*. Pellets were resuspended in 50 μl of water and used for X-ray diffraction measurements. The supernatant was passed through a 0.22 μm filter and its protein concentration was analysed by SDS–PAGE (NuPAGE, 4–12% Bis-Tris, Invitrogen) and the bicinchoninic acid (BCA) assay (Pierce).

Congo red binding

Congo red binding assays were performed as described previously[16] by using a Cary 4 UV–Vis spectrophotometer.

Electron microscopy

Samples were applied to Formvar-coated nickel grids, stained with 2% (w/v) uranyl acetate solution and viewed in a Phillips CEM100 transmission electron microscope operating at 80 kV.

X-ray fibre diffraction

Samples were prepared by air-drying fibril preparations between two waxed-filled capillary ends, aligned in the X-ray beam. Diffraction images were collected with a Rigaku Cu Kα rotating-anode source (wavelength 1.54 Å) and an R-Axis IV image-plate X-ray detector.

Mass spectrometry

Pulse labelling experiments, which involved the replacement of deuterium atoms with hydrogen atoms from the solvent H_2O, were done with D67H lysozyme that had initially been deuterated at all the labile exchangeable sites and a Bio-Logic QFM5 mixer, as described previously[11]. The samples that were allowed to exchange for more than 2 min were prepared by manual mixing. For the experiments in the presence of an equimolar amount of cAb-HuL6, deuterated D67H lysozyme and protonated cAb-HuL6 were mixed immediately before the experiment was performed. Exchange was done at pH 8.0 (100 mM ammonia/formic acid in H_2O) and 37 °C for various lengths of time and then quenched by decreasing the temperature and pH. The samples were electrosprayed at the base pressure of the Platform mass spectrometer (Micromass) and at a cone voltage of 150 V, where the complex between the antibody fragment and the lysozyme was found to dissociate. Mass spectra shown in Fig. 2 represent the convolution of the +8, +9, +10 charge states with minimal smoothing and converted to a mass scale.

Crystal structure determination

Crystals of cAb-HuL6 complexed with wild-type lysozyme were grown by the hanging drop vapour diffusion method at 20 °C. Drops initially contained equal volumes of protein (0.2 mM in buffer) and reservoir buffer (20% w/v PEG 4000 and 0.2 M imidazole malate, pH 6.0). Details of the data collection and processing will be described elsewhere (Decanniere *et al.*, manuscript in preparation). The atomic coordinates have been deposited in the Protein Data Bank (accession number 1OP9).

NMR spectroscopy

Two-dimensional gradient-enhanced ^{15}N-^{1}H HSQC spectra of unbound wild-type and D67H lysozyme, and of the proteins complexed with cAb-HuL6, were collected at 750 MHz at 35 °C. The samples of the complexes were made up with ~0.6 and ~0.4 mM ^{15}N-labelled wild-type and D67H lysozyme, respectively, and with a ~20% excess of unlabelled cAb-HuL6, to ensure all the lysozyme was bound in the complex, at pH 6.5 in 20 mM phosphate buffer in 95% H_2O/5% D_2O. The HSQC spectra were collected with 64 transients per t_1 increment, with 128 and 1024 complex points in t_1 and t_2, and with sweep widths of 10,582 and 2,273 Hz in F_2 and F_1. The ^{1}H and ^{15}N resonances of wild-type

lysozyme in the complex were assigned by using a ^{15}N-edited three-dimensional nuclear Overhauser enhancement (NOE) spectroscopy—HSQC experiment. This was collected with eight transients per increment, with 128, 28 and 512 complex points in t_1 (^{1}H), t_2 (^{15}N) and t_3 (^{1}H), and with acquisition times of 14.2, 12.3 and 48.4 ms in t_1, t_2 and t_3. The observed NOE data for bound lysozyme were interpreted by using published assignments for the free protein[29]. The resonances of D67H were assigned by comparison with the assigned spectrum of the unbound protein[11] and that of the wild-type complex.

Received 22 March; accepted 18 June 2003; doi:10.1038/nature01870.

1. Tan, S. Y. & Pepys, M. Amyloidosis. *Histopathology* **25,** 403–414 (1994).
2. Koo, E. H., Lansbury, P. T. Jr & Kelly, J. W. Amyloid diseases: Abnormal protein aggregation in neurodegeneration. *Proc. Natl Acad. Sci. USA* **96,** 9989–9990 (1999).
3. Dobson, C. M. The structural basis of protein folding and its links with human disease. *Phil. Trans. R. Soc. Lond. B* **356,** 133–145 (2001).
4. Pepys, M. B. *et al.* Human lysozyme gene mutations cause hereditary systemic amyloidosis. *Nature* **362,** 553–557 (1993).
5. Valleix, S. *et al.* Hereditary renal amyloidosis caused by a new variant lysozyme W64R in a French family. *Kidney Int.* **61,** 907–912 (2002).
6. Yazaki, M., Farrell, S. A. & Benson, M. D. A novel lysozyme mutation Phe57Ile associated with hereditary renal amyloidosis. *Kidney Int.* **63,** 1652–1657 (2003).
7. Dumoulin, M. *et al.* Single-domain antibody fragments with high conformational stability. *Protein Sci.* **11,** 500–515 (2002).
8. Hamers-Casterman, C. *et al.* Naturally occurring antibodies devoid of light chains. *Nature* **363,** 446–448 (1993).
9. Muyldermans, S. Single domain camel antibodies: current status. *J Biotechnol.* **74,** 277–302 (2001).
10. Booth, D. R. *et al.* Instability, unfolding and aggregation of human lysozyme variants underlying amyloid fibrillogenesis. *Nature* **385,** 787–793 (1997).
11. Canet, D. *et al.* Local cooperativity in the unfolding of an amyloidogenic variant of human lysozyme. *Nature Struct. Biol.* **9,** 308–315 (2002).
12. Schenk, D. Amyloid-beta immunotherapy for Alzheimer's disease: the end of the beginning. *Nature Rev. Neurosci.* **3,** 824–828 (2002).
13. Peretz, D. *et al.* Antibodies inhibit prion propagation and clear cell cultures of prion infectivity. *Nature* **412,** 739–743 (2001).
14. White, A. R. *et al.* Monoclonal antibodies inhibit prion replication and delay the development of prion disease. *Nature* **422,** 80–83 (2003).
15. Harper, J. D. & Lansbury, P. T. Jr Models of amyloid seeding in Alzheimer's disease and scrapie: mechanistic truths and physiological consequences of the time-dependent solubility of amyloid proteins. *Annu. Rev. Biochem.* **66,** 385–407 (1997).
16. Klunk, W. E., Pettegrew, J. W. & Abraham, D. J. Two simple methods for quantifying low-affinity dye-substrate binding. *J. Histochem. Cytochem.* **37,** 1293–1297 (1989).
17. Colon, W. & Kelly, J. W. Partial denaturation of transthyretin is sufficient for amyloid fibril formation in vitro. *Biochemistry* **31,** 8654–8660 (1992).
18. Morozova-Roche, L. A. *et al.* Amyloid fibril formation and seeding by wild-type human lysozyme and its disease-related mutational variants. *J. Struct. Biol.* **130,** 339–351 (2000).
19. Sunde, M. *et al.* Common core structure of amyloid fibrils by synchrotron X-ray diffraction. *J. Mol. Biol.* **273,** 729–739 (1997).
20. Aguzzi, A., Glatzel, M., Montrasio, F., Prinz, M. & Heppner, F. L. Interventional strategies against prion diseases. *Nature Rev. Neurosci.* **2,** 745–749 (2001).
21. Wolfe, M. S. Therapeutic strategies for Alzheimer's disease. *Nature Rev. Drug Discov.* **1,** 859–866 (2002).
22. Pepys, M. B. *et al.* Targeted pharmacological depletion of serum amyloid P component for treatment of human amyloidosis. *Nature* **417,** 254–259 (2002).
23. Dobson, C. M. Protein folding and disease: a view from the first Horizon Symposium. *Nature Rev. Drug Discov.* **2,** 154–160 (2003).
24. May, B. C. *et al.* Potent inhibition of scrapie prion replication in cultured cells by bis-acridines. *Proc. Natl Acad. Sci. USA* **100,** 3416–3421 (2003).
25. McCammon, M. G. *et al.* Screening transthyretin amyloid fibril inhibitors. Characterization of novel multiprotein, multiligand complexes by mass spectrometry. *Structure (Cambridge)* **10,** 851–863 (2002).
26. Hammarstrom, P., Wiseman, R. L., Powers, E. T. & Kelly, J. W. Prevention of transthyretin amyloid disease by changing protein misfolding energetics. *Science* **299,** 713–716 (2003).
27. Branden, C. & Tooze, J. *Introduction to Protein Structure* (Garland, New York, 1999).
28. Spencer, A. *et al.* Expression, purification, and characterization of the recombinant calcium-binding equine lysozyme secreted by the filamentous fungus *Aspergillus niger*: Comparisons with the production of hen and human lysozymes. *Protein Expr. Purif.* **16,** 171–180 (1999).
29. Ohkubo, T., Taniyama, Y. & Kikuchi, M. 1H and 15N NMR study of human lysozyme. *J. Biochem. (Tokyo)* **110,** 1022–1029 (1991).
30. Koradi, R., Billeter, M. & Wuthrich, K. MOLMOL: a program for display and analysis of macromolecular structures. *J. Mol. Graph.* **14,** 51–55 (1996).

Acknowledgements The assistance of J. Zurdo, M. Krebs and B. Luisi for TEM and X-diffraction analysis of fibrils is gratefully acknowledged. We thank J.-M. Frère for many discussions. M.D. and D.C. were supported by a fellowship from the European Community. G.L. was supported by a fellowship from the Wenner-Gren Foundation. C.R. was supported by a BBSRC Advanced Research Fellowship. A.M. is a Research Associate of the FNRS, and was supported in part by a grant from the FRFC. C.V.R. is a Royal Society University Research Fellow. The research of C.M.D. is supported in part by a Programme Grant from the Wellcome Trust. This work was also supported by a BBSRC grant (to C.M.D., C.V.R. and D.B.A.) and by the Belgian Government through the PAI.

Competing interests statement The authors declare that they have no competing financial interests.

Correspondence and requests for materials should be addressed to C.M.D. (cmd44@cam.ac.uk).

Comparative analyses of multi-species sequences from targeted genomic regions

J. W. Thomas[1]*, J. W. Touchman[1,2]*, R. W. Blakesley[1,2], G. G. Bouffard[1,2], S. M. Beckstrom-Sternberg[1,2], E. H. Margulies[1], M. Blanchette[3], A. C. Siepel[3], P. J. Thomas[2], J. C. McDowell[2], B. Maskeri[2], N. F. Hansen[2], M. S. Schwartz[3], R. J. Weber[3], W. J. Kent[3], D. Karolchik[3], T. C. Bruen[3], R. Bevan[3], D. J. Cutler[4], S. Schwartz[5], L. Elnitski[5], J. R. Idol[1], A. B. Prasad[1], S.-Q. Lee-Lin[1], V. V. B. Maduro[1], T. J. Summers[1], M. E. Portnoy[1], N. L. Dietrich[2], N. Akhter[2], K. Ayele[2], B. Benjamin[2], K. Cariaga[2], C. P. Brinkley[2], S. Y. Brooks[2], S. Granite[2], X. Guan[2], J. Gupta[2], P. Haghighi[2], S.-L. Ho[2], M. C. Huang[2], E. Karlins[2], P. L. Laric[2], R. Legaspi[2], M. J. Lim[2], Q. L. Maduro[2], C. A. Masiello[2], S. D. Mastrian[2], J. C. McCloskey[2], R. Pearson[2], S. Stantripop[2], E. E. Tiongson[2], J. T. Tran[2], C. Tsurgeon[2], J. L. Vogt[2], M. A. Walker[2], K. D. Wetherby[2], L. S. Wiggins[2], A. C. Young[2], L.-H. Zhang[2], K. Osoegawa[6], B. Zhu[6], B. Zhao[6], C. L. Shu[6], P. J. De Jong[6], C. E. Lawrence[7], A. F. Smit[8], A. Chakravarti[4], D. Haussler[3,9], P. Green[10], W. Miller[5] & E. D. Green[1,2]

[1]*Genome Technology Branch, National Human Genome Research Institute, and* [2]*NIH Intramural Sequencing Center, National Institutes of Health, Bethesda, Maryland 20892, USA*
[3]*Center for Biomolecular Science and Engineering, University of California, Santa Cruz, California 95064, USA*
[4]*Institute of Genetic Medicine, Johns Hopkins University School of Medicine, Baltimore, Maryland 21287, USA*
[5]*Department of Computer Science and Engineering, The Pennsylvania State University, University Park, Pennsylvania 16802, USA*
[6]*Children's Hospital Oakland Research Institute, Oakland, California 94609, USA*
[7]*The Wadsworth Center for Laboratories and Research, New York State Department of Health, Albany, New York 12201, USA*
[8]*The Institute for Systems Biology, Seattle, Washington 98103, USA*
[9]*Howard Hughes Medical Institute, University of California, Santa Cruz, California 95064, USA*
[10]*Howard Hughes Medical Institute and Department of Genome Sciences, University of Washington, Seattle, Washington 98195, USA*

* Present addresses: Department of Human Genetics, Emory University School of Medicine, Atlanta, Georgia 30322, USA (J.W.Th.); Translational Genomics Research Institute, Phoenix, Arizona 85004 and Department of Biology, Arizona State University, Tempe, Arizona 85287, USA (J.W.To.)

The systematic comparison of genomic sequences from different organisms represents a central focus of contemporary genome analysis. Comparative analyses of vertebrate sequences can identify coding[1–6] and conserved non-coding[4,6,7] regions, including regulatory elements[8–10], and provide insight into the forces that have rendered modern-day genomes[6]. As a complement to whole-genome sequencing efforts[3,5,6], we are sequencing and comparing targeted genomic regions in multiple, evolutionarily diverse vertebrates. Here we report the generation and analysis of over 12 megabases (Mb) of sequence from 12 species, all derived from the genomic region orthologous to a segment of about 1.8 Mb on human chromosome 7 containing ten genes, including the gene mutated in cystic fibrosis. These sequences show conservation reflecting both functional constraints and the neutral mutational events that shaped this genomic region. In particular, we identify substantial numbers of conserved non-coding segments beyond those previously identified experimentally, most of which are not detectable by pair-wise sequence comparisons alone. Analysis of transposable element insertions highlights the variation in genome dynamics among these species and confirms the placement of rodents as a sister group to the primates.

The NIH Intramural Sequencing Center (NISC) Comparative Sequencing Program aims to sequence and to analyse targeted genomic regions in multiple vertebrates. Our initial target is a genomic segment of about 1.8 Mb on human chromosome 7q31.3